Appl. Phys. B (2015) 121:459–464
DOI 10.1007/s00340-015-6253-3

Applied Physics B
Lasers and Optics

Characterization of single coal particle combustion within oxygen-enriched environments using high-speed OH-PLIF

J. Köser[1] · L. G. Becker[1] · N. Vorobiev[2] · M. Schiemann[2] · V. Scherer[2] · B. Böhm[3] · A. Dreizler[1]

Received: 13 August 2015 / Accepted: 15 October 2015 / Published online: 30 October 2015
© Springer-Verlag Berlin Heidelberg 2015

Abstract This work presents first-of-its-kind high-speed planar laser-induced fluorescence measurements of the hydroxyl radical in the boundary layer of single coal particles. Experiments were performed in a laminar flow reactor providing an oxygen-enriched exhaust gas environment at elevated temperatures. Single coal particles in a sieve fraction of 90–125 µm and a significant amount of volatiles (36 wt%) were injected along the burner's centerline. Coherent anti-Stokes Raman spectroscopy measurements were taken to characterize the gas-phase temperature. Time-resolved imaging of the OH distribution at 10 kHz allowed identifying reaction and post-flame zones and gave access to the temporal evolution of burning coal particles. During volatile combustion, a symmetric diffusion flame was observed around the particle starting from a distance of ~150 µm from the particle surface. For subsequent char combustion, this distance decreased and the highest OH signals appeared close to the particle surface.

1 Introduction

Coal is one of the most important primary energy carriers for power generation. On the one hand, coal combustion is expected to further increase, and on the other hand, man-made emissions of the greenhouse gas carbon dioxide (CO_2), which are a likely cause for the ongoing climate change, need to be reduced [1]. Effective strategies for CO_2 reduction and/or capture and storage (CCS) need to be explored. This requires deeper insight into the underlying chemical and physical phenomena of coal combustion as a basis for advanced methods and tools for the development process of new combustion technologies. Investigating ignition and combustion of coal particles is important to improve our understanding as a prerequisite for developing mathematical combustion models.

Typical pulverized coal combustion conditions imply small particles (≤100 µm) and high furnace temperatures (~1500 K gas temperature) resulting in high heating rates of the particles in the range of 10^4–10^5 K/s [2–4]. Under these conditions, ignition of the volatile matter surrounding a devolatilizing particle, ignition of the char surface or a combination of both can occur [5–7]. Mass transport processes in the boundary layer can limit burning rates which is addressed by several models [8–11]. Depending on the model, calculated burning rates can vary substantially, affecting predicted efficiencies of pulverized coal boilers. Furthermore, ignition and combustion of coal particles sensitively depend on the surrounding atmosphere, especially in case of oxyfuel combustion, where air is replaced by oxygen and recirculated exhaust gas, containing high amounts of CO_2 and partially H_2O. Oxyfuel combustion does have a high potential for efficient capture and sequestration of CO_2.

For a fundamental investigation of coal ignition and combustion processes, laminar flow reactors are used regularly providing an oxygen-enriched exhaust gas environment at high temperatures where single coal particles are introduced [12–16]. For in situ and noninvasive

✉ J. Köser
koeser@csi.tu-darmstadt.de

[1] Fachgebiet Reaktive Strömungen und Messtechnik, Technische Universität Darmstadt, Jovanka-Bontschits-Straße 2, 64287 Darmstadt, Germany

[2] Department of Energy Plant Technology, Ruhr-University, Universitätsstraße 150, 44801 Bochum, Germany

[3] Fachgebiet Energie- und Kraftwerkstechnik, Technische Universität Darmstadt, Jovanka-Bontschits-Straße 2, 64287 Darmstadt, Germany

measurements, optical diagnostics have been applied to these configurations. Particle temperatures were measured using two- or three-color pyrometry [17, 18], particle size was measured by an extended stereoscopic pyrometer [19], or flame luminosity was recorded to visualize ignition and determine the duration of volatile combustion [12, 14, 16, 20]. Recording of CH* was exploited to characterize the onset of ignition and duration of volatile combustion, which was found to be a better indicator than blackbody emission from soot or hot char [12]. Unfortunately, the CH* signal is weak and has a strong spectral overlap with broadband blackbody emission.

Laser-induced fluorescence (LIF) of the hydroxyl (OH) radical is widely used to visualize reaction zones in gaseous flames [21]. In case of two-phase flows, particles do not impede OH-LIF signals significantly. Therefore, OH-LIF has already been applied successfully to study global structures of gas-assisted coal flames [22–24].

In this paper, we report on planar OH-LIF as a suitable method for investigating ignition and combustion of single coal particles. A high-speed LIF system was used to temporally track the evolution of ignition and combustion processes by visualizing OH radicals in the particle boundary layer. Selected results are presented and discussed to demonstrate the feasibility and to highlight the potentials of this method.

2 Experimental setup

2.1 Laminar flow reactor

The experiments were carried out in a laminar flow reactor based on a nonpremixed Hencken burner design enclosed by a quadratic quartz glass chimney [25]. A sketch of the burner is shown in Fig. 1. Methane diluted with N_2 was injected through 100 hypodermic tubes evenly distributed (mean distance 4.5 mm) over the 5 × 5 cm^2 plate into a nitrogen/oxygen mixture serving as oxidizer. A ceramic honeycomb with ~400 rectangular holes (2 × 2 mm^2) was used to hold the fuel tubes in position and to distribute the oxidizer homogenously. The burner's surface is defined as height zero in this work. At the investigated operating point (41.8 sl/min air, 3.6 sl/min CH_4, 9.4 sl/min O_2, 5 sl/min N_2), the resulting exhaust gas composition was 20 vol% oxygen, 59 vol% nitrogen, 7 vol% carbon dioxide and 14 vol% of steam. The total volume flow is 60 sl/min. Single coal particles were injected through a central tube with an inner diameter of 2 mm using nitrogen as carrier gas with a flow rate of 0.2 sl/min. The seeding density was kept low to provide single isolated burning particles. A typical bituminous power plant coal from Colombia (Norte) was used containing 3 wt% moisture, 8.5 wt% ash

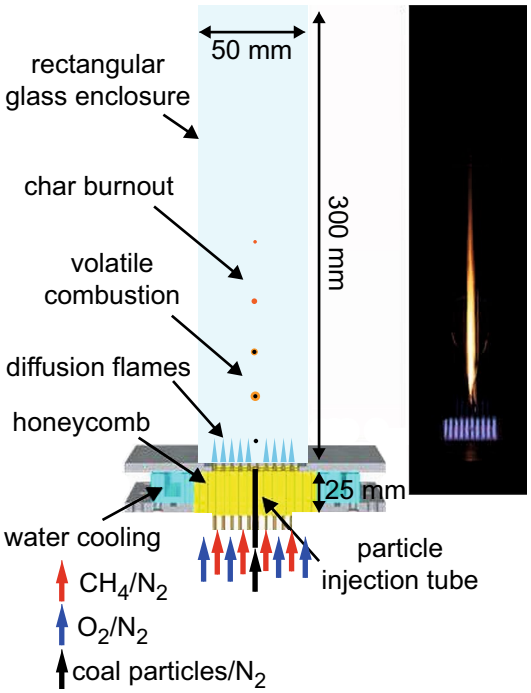

Fig. 1 Schematic of the flow reactor (*left*) and a photograph showing a typical streak of burning coal particles (*right*)

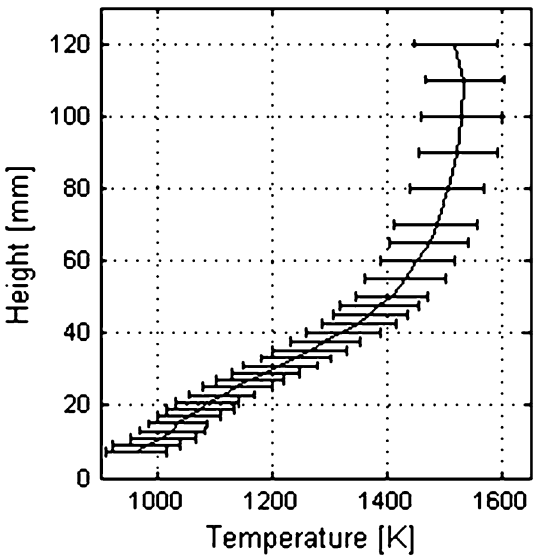

Fig. 2 Mean and standard deviation of gas temperature profile along the burner's centerline obtained from CARS measurements

and 36 wt% volatiles (as delivered). Particles were sieved to a size range of 90–125 µm.

In a first step, gas-phase temperatures as most important boundary conditions for igniting coal particles were measured, using conventional nanosecond ro-vibrational coherent anti-Stokes Raman spectroscopy (CARS) of N_2.

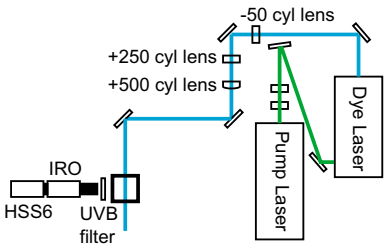

Fig. 3 Sketch of the experimental setup used for high-speed OH-PLIF

A horizontally aligned planar BOXCARS phase matching was used with a resulting probe volume of 65 µm in diameter and 1.5 mm in length. For details, we refer to [26]. For the selected operation point, mean and standard deviations of local gas temperatures along the burner's centerline are shown in Fig. 2. The temperature rise along the centerline results from mixing of the inert particle carrier gas with the surrounding hot exhaust gas. Notice that no coal particles were present in the carrier gas during the CARS measurement.

2.2 High-speed planar laser-induced fluorescence of OH

The optical setup for the planar OH-LIF was similar to that used by [27] and is shown in Fig. 3. A frequency-doubled dye laser (Sirah Credo, with Rhodamine 6G) pumped at 532 nm by a frequency-doubled, Q-switched diode-pumped solid-state laser (Edgewave IS8II-E) was used to produce UV pulses of 0.28 mJ at 10 kHz. The laser was tuned to 282.92 nm to excite the $Q_1(6)$ line of the A-X (1-0) transition of OH. A laser sheet was formed using a combination of three cylindrical lenses resulting in a 100-µm-thick sheet with a height of 10 mm. Fluorescence was detected at 310 nm using a CMOS camera (HSS6, LaVision) equipped with a two-stage, lens-coupled intensifier (HS-IRO, LaVision), a UV-achromat lens (Halle, $f = 150$ mm, f/2.5) and a 30-nm bandwidth filter centered at 300 nm. The IRO gate was set to 100 ns suppressing flame luminosity, chemiluminescence of OH* and near-IR radiation of the particle. The field of view extended over 18 × 18 mm. Subsequent to correction for an inhomogeneous laser sheet profile and pulse-to-pulse energy variations, a 3 × 3 pixel Gaussian smoothing filter was applied to the images to remove noise at spatial scales near the optical resolution limit of the PLIF setup of 4.5 px determined by a Siemens star. For high-speed measurements, additional particle heating due to laser excitation needs to be considered. The coal particles were exposed to ~30 laser excitations while moving through the 10-mm-high laser sheet. Assuming 100 % laser absorption and no heat losses from the particle to the surrounding, particle heating was estimated to be <2.5 K per laser pulse.

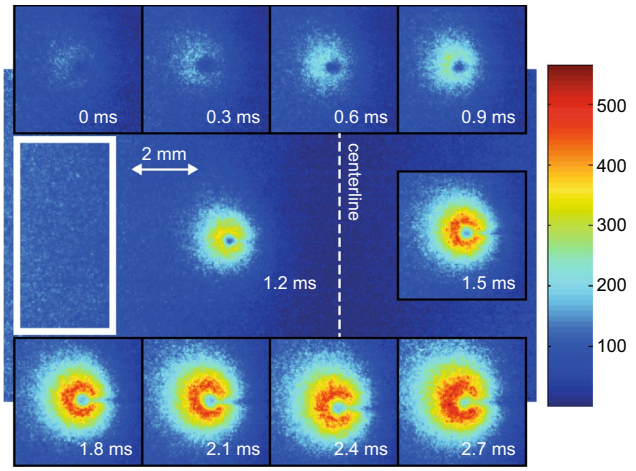

Fig. 4 OH-PLIF images taken at 10 kHz of an igniting coal particle (every third image shown) centered at the burners *centerline* at a height of 15 ± 5 mm

3 Results and discussion

Figure 4 shows the temporal evolution of the instantaneous OH radical distribution in the vicinity of an individual coal particle just after ignition and during combustion of volatiles (every third image shown). This sequence is recorded along the centerline with the field of view centered at 15 mm above the burner's exit. The homogenously distributed OH background (left side of the central enlarged image) results from dissociation reactions of hot water vapor present in the exhaust gas of the Hencken-type burner. The region of lower OH background signals in the center of the image is a result of mixing between the cold inert particle carrier gas and hot exhaust gases. The signal-to-noise ratio (SNR) was estimated using data from the inserted white box (100 × 200 pixels) within the homogenously distributed OH region. Noise is quantified here as the spatial standard deviation. For the region of background OH, a SNR of 6 is obtained, whereas the peak OH signals of the diffusion flame surrounding the coal particle are ~10 times higher than the mean of the white box. Signal contributions due to laser scattering were determined by detuning the dye laser off the molecular resonance. Signal levels up to 30 counts were found at the location of the particle, while no significant contributions were observed in the immediate surrounding of the particle where coal combustion occurs.

The onset of ignition ($t = 0$ ms) is defined by that frame where an increase in OH signals beyond the background

level was observed first. Subsequently, the OH signal level continuously increases for the next 1.5 ms. The OH distribution around the igniting particle forms a concentric symmetric shell that appears as a ring due to the two-dimensional nature of the LIF measurements. The low OH signals in the region where the particle is found and the dark streak observed to the right of the particle indicate that the 100-µm-thick collimated laser sheet (coming from left) hits the particle approximately centrally. Even in case that the laser sheet was slightly offset relative to the particle's center, a ring will be observed because volatiles outgassing from the particle generate a fuel-rich zone outside the flammability limits that extends the sheet thickness of 100 µm (see discussion below). The central region exhibits a nonzero OH signal level which is attributed to a slight out-of-plane offset of the particle relative to the laser sheet, remaining laser scattering off the particle and to the blurring of the IRO. This is a well-known phenomenon of two-stage image intensifiers [28].

For improving SNR radial, OH profiles were averaged circumferentially over the left hemisphere of the shell surrounding the particle. Results are shown in Fig. 5 (every third image shown) using the same sequence as in Fig. 4. The vertical dashed line at a distance from the particle center $r = 0.055$ mm indicates the mean diameter of the unburned coal particle. Once the particle enters the laser sheet (0 ms), a central minimum forms due to the presence of the particle and the outgassing volatiles forming a shell of gaseous fuel around the particle. A slight increase in OH signals is observed beyond $r = 0.1$ mm where the volatiles mix with the oxygen from the hot exhaust gases. Most probably in this region, auto-ignition starts, forming a local maximum at $r = 0.5$ mm for $t = 0$ ms. Within 1 ms, the maximum OH signal continuously increases and shifts closer toward the particle ($r = 0.3$ mm) leading to a steeper OH gradient. This is attributed to the formation of a gaseous diffusion flame forming in the mixing layer around the coal particle that is fed by the outgassing volatiles. For later times, the trend reverses and the OH peak moves outwards. At 2 ms, the OH peak is located at $r = 0.4$ mm. Although we can only speculate on possible reasons, this slight shift might be caused by an increased outgassing rate (due to increased particle temperature, which leads to increasing pyrolysis rates) once the volatile combustion starts. This would involve an increased momentum of volatiles pushing the reaction zone to larger distances from the particle center. However, during volatile combustion, a significant gap of at least 0.15 mm remains between particle surface and reaction zone.

Different phases of coal combustion are explored by high-speed OH-PLIF measurements at different heights above the burner. For this purpose, a total of three field of views are selected that are centered axially around 15, 30, and 75 mm. Subsequent to pyrolysis and outgassing of volatiles that is associated with a diffusion flame, char combustion starts. Char combustion constitutes heterogeneous reactions at the particle surfaces. In a laminar flow reactor, char combustion appears at larger heights above the burner than volatile combustion. Figure 6 shows circumferentially averaged OH profiles at these selected heights. Thin lines represent profiles of individual particles, whereas the bold line is the ensemble average. From approximately 50 sequences recorded at each height, only those were selected where the laser sheet hits the particle and where combustion was observed. Only one image is used from each selected sequence. The length of the radial profiles depends on the horizontal position of each particle within the field of view. Notice that each image was corrected for its laser pulse energy such that relative LIF signal strength can be compared.

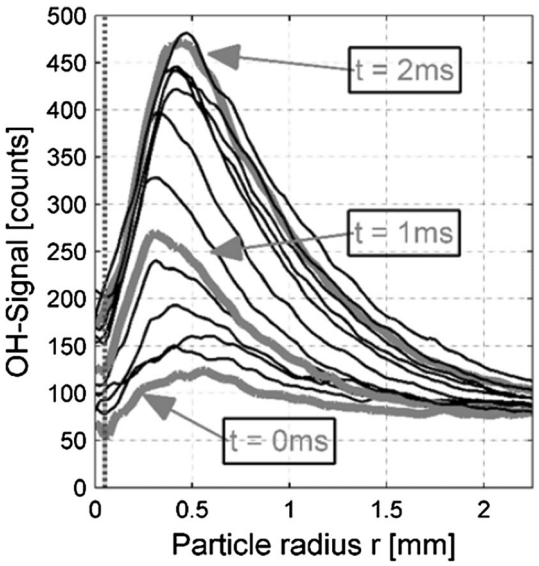

Fig. 5 Radial OH profiles averaged circumferentially across the left hemisphere of the particle shown in Fig. 4. The sequence shows (every third profile shown) the transition from an instant right after ignition to a fully developed diffusion flame surrounding the particle. *Vertical dashed line* at 0.055 mm indicates the mean diameter of the unburned coal particle

At 15 mm, the scatter of the profiles reveals that the elapsed time from ignition varies for individual particles. Only one of the observed particles already reaches a peak OH signal level (~500 counts) representative for a fully developed diffusion flame (see Figs. 4, 5). All other events display lower intensities associated with a transition from ignition to a diffusion flame. At 30 mm, the scatter reduces, OH signal levels are in average ~20 % higher compared to 15 mm, and OH at high concentrations is located closer to the particle surface. This is an indication that diffusion flames surrounding each particle are fully developed.

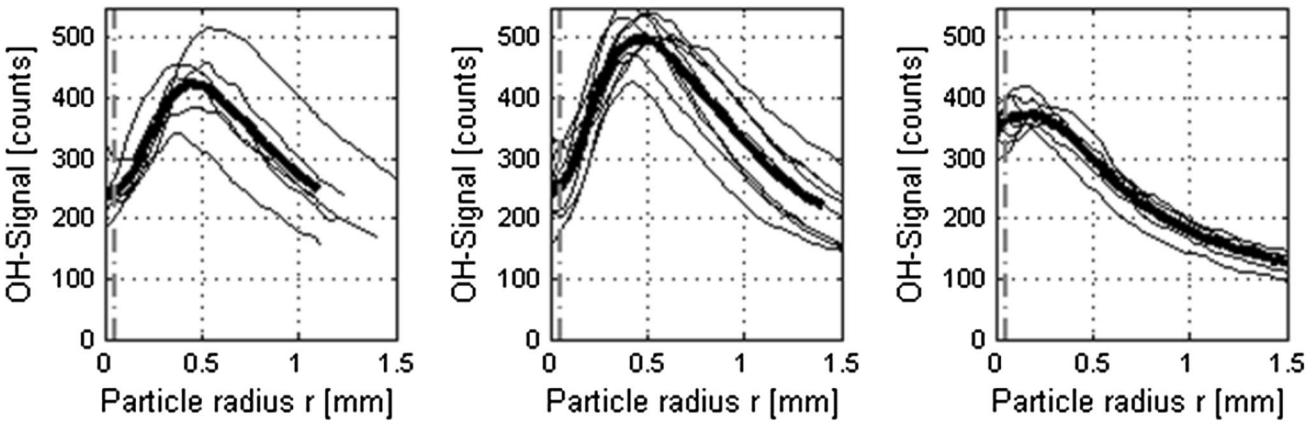

Fig. 6 Circumferentially averaged OH profiles of individual burning particles (*thin gray lines*) for a height of 15 mm (*left*, 6 events), 30 mm (*middle*, 9 events) and 75 mm (*right*, 7 events). The ensemble mean is represented by the *bold black line*

Compared to the 15-mm position, much less particles are observed that not yet have undergone auto-ignition. It has to be noted that ignition is size dependent, such that larger particles tend to show delayed ignition, and thus, the spread in ignition time can be attributed to the particle size distribution.

At 75 mm, a significant change in the flame structure is observed. The steepest OH gradient is found close by the position of the initial mean particle radius at $r \approx 0.055$ mm. Additionally, the scatter between individual events further reduces. This phase is attributed to char combustion. Outgassing of the volatiles is completed, and exothermal surface reactions occur. During this phase, the C/H ratio increases. Thus, OH produced from char combustion decreases compared to the phase of volatile combustion. During char combustion, particle temperatures reach up to 2400 K under the given conditions, investigated in [19], which is far above mean temperatures of the surrounding exhaust gas of ~1500 K (compare Fig. 2). With increasing temperature, the chemical equilibrium is shifted from water toward OH. Furthermore, gasification reactions of the char surface involving CO_2 and H_2O affect the boundary layer concentration [8, 29], producing CO and H_2 with the CO predominantly produced by the oxidation reaction under these conditions [30]. These chemical species are transported away from the particle surface. Additionally, the homogeneous water gas shift reaction leads to a further source of H_2, which can react with O_2 to OH in the particle boundary layer. With increasing distance from the particle, the influence of H_2 from gasification reactions shrinks and temperatures approach those of the surrounding gas. This causes a decrease in the OH-LIF signal for radial positions larger than ~0.4 mm. All of these interconnected transport and reaction processes produce OH forming a shell that was observed in our experiments.

4 Conclusions

For the first time, time-resolved planar laser-induced fluorescence measurements were taken at 10 kHz to image ignition and combustion processes of single coal particles exposed to an oxygen-enriched exhaust gas environment at elevated temperatures. Gas temperatures were measured by CARS without particles being present. OH distributions appear as useful marker for identifying locations slightly after onset of ignition and for distinguishing volatile from char combustion.

Acknowledgments The authors gratefully acknowledge the sponsorship of the Deutsche Forschungsgemeinschaft through SFB/TRR 129, subprojects A02 and B05. A. Dreizler is grateful for generous support through the Gottfried Wilhelm Leibniz program of Deutsche Forschungsgemeinschaft.

References

1. B. Metz, O. Davidson, H.C. de Coninck, M. Loos, L.A. Meyer, *Carbon dioxide Capture and Storage* (Cambridge University Press, Cambridge, 2005)
2. H.-Y. Cai, Fuel **75**(1), 15–24 (1996)
3. R.H. Essenhigh, M.K. Misra, D.W. Shaw, Combust. Flame **77**, 3–30 (1989)
4. R.C. Shurtz, K.K. Kolste, T.H. Fletcher, Energy Fuels **25**, 2163–2173 (2011)
5. Y. Liu, M. Geier, A. Molina, C.R. Shaddix, Int. J. Greenh. Gas Control **5**, S36–S46 (2011)
6. R. Khatami, C. Stivers, Y.A. Levendis, Combust. Flame **159**, 3554–3568 (2012)
7. B. Goshayeshi, J.C. Sutherland, Combust. Flame **161**, 1900–1910 (2014)
8. E.S. Hecht, C.R. Shaddix, J.S. Lighty, Combust. Flame **160**, 1499–1509 (2013)
9. M. Geier, C.R. Shaddix, K.A. Davis, H.-S. Shim, Appl. Energy **93**, 675–679 (2012)
10. R.E. Mitchell, R.J. Kee, P. Glarborg, M.E. Coltrin, Proc. Combust. Inst. **23**(1), 1169–1176 (1991)

11. C. Gonzalo-Tirado, S. Jiménez, R. Johansson, J. Ballester, Combust. Flame **161**, 1085–1095 (2014)
12. A. Molina, C.R. Shaddix, Proc. Combust. Inst. **31**, 1905–1912 (2007)
13. A. Molina, J.J. Murphy, C.R. Shaddix, L.G. Blevins, Proc. Combust. Inst. **30**, 2187–2195 (2005)
14. C.R. Shaddix, A. Molina, Proc. Combust. Inst. **32**, 2091–2098 (2009)
15. M. Taniguchi, H. Okazaki, H. Kobayashi, S. Azuhata, H. Miyadera, H. Muto, T. Tsumura, J. Energy Resour. Technol. **123**, 32 (2001)
16. H. Lee, S. Choi, Combust. Flame **162**, 2610–2620 (2015)
17. P.A. Bejarano, Y.A. Levendis, Combust. Flame **153**, 270–287 (2008)
18. M. Schiemann, V. Scherer, S. Wirtz, Chem. Eng. Technol. **32**, 2000–2004 (2009)
19. M. Schiemann, N. Vorobiev, V. Scherer, Appl. Opt. **54**, 1097 (2015)
20. L. Zhang, E. Binner, Y. Qiao, C.-Z. Li, Energy Fuels **24**, 29–37 (2010)
21. E.P. Hassel, S. Linow, Meas. Sci. Technol. **11**, R37 (2000)
22. S. Balusamy, M.M. Kamal, S.M. Lowe, B. Tian, Y. Gao, S. Hochgreb. Exp. Fluids **56**, 108 (2015)
23. S.M. Hwang, R. Kurose, F. Akamatsu, H. Tsuji, H. Makino, M. Katsuki, Energy Fuels **19**, 382–392 (2005)
24. N. Darabiha, P. Scouflaire, M. Xia, B. Fiorina, in *ECM* (2015)
25. N. Vorobiev, M. Schiemann, in *40th International Technical Conference on Clean Coal Fuel System*, Clearwater, Florida, USA (2015), pp. 550–561
26. A. Singh, M. Mann, T. Kissel, J. Brübach, A. Dreizler, Flow Turbul. Combust. **90**, 723–739 (2013)
27. P.J. Trunk, I. Boxx, C. Heeger, W. Meier, B. Böhm, A. Dreizler, Proc. Combust. Inst. **34**, 3565–3572 (2013)
28. R.L. Gordon, C. Heeger, A. Dreizler, Appl. Phys. B **96**, 745–748 (2009)
29. E.S. Hecht, C.R. Shaddix, M. Geier, A. Molina, B.S. Haynes, Combust. Flame **159**, 3437–3447 (2012)
30. L. Tognotti, J.P. Longwell, A.F. Sarofim, Proc. Combust. Inst. **23**, 1207–1213 (1991)